F. Carpignano, G. Rigamonti, T. Migliazza, S. Merlo, **Refractive index sensing in rectangular glass micro-capillaries by spectral reflectivity measurements**, *IEEE Journal of Selected Topics in Quantum Electronics* (Special Issue on Biophotonics, 2016), Vol. 22, No. 3, pp. 7100309_1-7100309_9, Piscataway, NJ, USA (2016). DOI: 10.1109/JSTQE.2015.2455339

Refractive index sensing in rectangular glass micro-capillaries by spectral reflectivity measurements

Francesca Carpignano, Giulia Rigamonti, Tommaso Migliazza,
and Sabina Merlo, *Senior Member*, *IEEE*

***Abstract*—We report the application of rectangular glass micro-capillaries with cross-section of 20 μm x 200 μm and 50 μm x 500 μm as capillary-driven liquid-core optical cavities for fluid refractive index sensing. Reflected power spectra in two wavelength bands (around 1.3 μm and 1.55 μm) are detected with readout broadband radiation crossing the capillary in orthogonal direction with respect to the flat sides. Using a fiberoptic scheme for remote, non-contact measurements and inserting glucose or bovine serum albumin solutions in water at different concentrations as test fluids, we have revealed the shift of the wavelength position of the reflectivity minima due to refractive index variations. The combination of these low-cost devices with a spectral readout method allows achieving sensitivities higher than 250 nm/RIU and limits of detection better than $1.3 \cdot 10^{-3}$ RIU.**

***Index Terms*—Reflectometry, Spectral measurements, Glass micro-capillary, Infrared radiation, Refractive index measurements.**

I. Introduction

WITH the synergistic integration of photonics and micro-fluidics, optical sensing is rapidly evolving from bulky systems to micro-opto-fluidic devices [1]–[5]. In biological and biochemical applications, in particular, miniaturization of analytical systems could have a great impact since it would allow to work with smaller sample volumes, reduce the response time, improve process control and realize portable instruments [6].

Among detection methods, label-free sensing (*i.e.*, without addition of exogenous markers) is very attractive since intrinsically less invasive, safer and potentially realizable at low-cost in terms of required reagents [6], [7]. Recently, increasing attention has been paid to optical label-free sensors that measure volumetric changes of refractive index (RI) of a homogeneous solution due to the presence of solutes with different RI from the solvent [4], [7], [8]. Optical label-free sensors are good candidates for lab-on-a-chip realizations as they allow the integration of both fluidic handling and optical analyses into a single chip. Detection of refractive index is well suited for micro-opto-fluidic sensors that have extremely small detection volumes (femtoliters to nanoliters) because the RI signal scales with the analyte bulk concentration, rather than with the total number of molecules, thus enabling ultralow quantities of molecules to be detected [4]. Various opto-fluidic architectures, including for example photonic crystals [9]–[16], resonant microcavities [7], [17], [18], micro-tube resonator [19] as well as interferometric structures such as ring resonators [20]–[29] and Fabry–Pérot cavities [30], [31] have been explored as ways for maximizing light-analyte interaction while satisfying other requirements of biological/chemical analysis. Typically, one or more optical resonant modes of the selected structure are monitored since the resonance conditions are modified when the RI of the tested sample changes [8], [25]. Resonances usually correspond to spectral reflectivity (or transmission) minima (or maxima) measured on the device. Therefore, the RI sample change is easily recognized from the shift of the wavelength position where the resonance occurs. The RI sensitivity can then be determined by dividing the wavelength shift by the defined RI variation.

To satisfy the increasing need of simple and low cost devices suitable for refractive index detection, there is a lot of interest in the use of glass micro-capillaries with rectangular cross-section that are commercially available in different dimensions [32]–[38].

Glass capillaries with rectangular cross-section are very useful when optical imaging from the top/bottom is desirable because their flat surfaces allow viewing the contents of the internal capillary with a microscope, at various magnifications. Optical distortions and scattering caused by the wall curvature of round cross-section capillary are strongly reduced in rectangular capillaries [32]. Evander et al. [34] employed glass capillaries with rectangular cross-section as the resonant part of a micro-fluidic system for acoustophoresis, a technology that exploits acoustic waves to move particles and cells without contact. Hammarstrom et al. [33] demonstrated the use of capillaries with rectangular cross-section as a pipette for aspirating, trapping and dispensing red blood cells. Tsuda et al. [32] used transparent rectangular

Manuscript received February 10, 2015; revised June 23, 2015. This work was partially funded by Fondazione CARIPLO, Grant no. 2011-0308.

F. Carpignano, G. Rigamonti, T. Migliazza and S. Merlo are with Dipartimento di Ingegneria Industriale e dell'Informazione, Università degli Studi di Pavia, 27100 Pavia, Italy (e-mail: carpignano@unipv.it, giulia.rigamonti01@universitadipavia.it, tommaso.migliazza02@universitadipavia.it, merlo@ieee.org).

Color versions of the figures in this paper are available online at http://ieeexplore.ieee.org.

Digital Object Identifier…

capillaries for capillary zone electrophoresis and they demonstrated that these devices were extremely efficient at dissipating heat compared to conventional circular capillaries.

A glass micro-capillary with rectangular cross-section can be viewed as a three-layer optical structure composed by two borosilicate glass walls separated by the inner gap [39], [40]. Optical readout using broadband radiation that crosses the device in direction orthogonal to the long, flat sides is based on the observation that the back-reflected signal exhibits wavelength intervals where reflectivity is high separated by deep reflectivity notches. The micro-capillary can be considered a liquid-core optical cavity since the solution under test may flow through the device. Therefore, the wavelength position of the reflectivity minima depends not only on the capillary size but also on the refractive index of the fluid filling the capillary channel. If the fluid RI is changed, a shift of the wavelength position of the minima is expected [8], [9], [41].

In this work, we are reporting the use of rectangular capillaries as micro-opto-fluidic devices combined with a spectral readout method for refractive index volume sensing. We tested two kinds of capillaries with 20-µm-deep and 200-µm-wide or with 50-µm-deep and 500-µm-wide inner core, indicated as 20-µm and 50-µm capillary, respectively. The glass wall thickness was nominally equal to the core depth. We investigated the reflected power spectra of these devices in the near infrared around 1.3 µm and 1.55 µm using glucose solutions and Bovine Serum Albumin (BSA) solutions in water, as test fluids. Capillary forces successfully achieved capillary core filling. By following the shift (induced by RI changes) of the detected deep notches in the reflected power spectra, we obtained experimental values of sensitivity of the order of 250-450 nm/RIU in agreement with the results of numerical simulations performed by modeling the capillary as a three-layer structure. Limits of detection for refractive index in the range 10^{-5} - 10^{-3} RIU (Refractive Index Unit) were also demonstrated. The reported scheme allows remote, non-contact measurements on the capillary that can also be easily replaced without affecting the optical setup.

II. Instrumental Configuration for Reflectivity Measurements

Fig. 1 shows a schematic of the experimental setup that we used to investigate the spectral reflectivity in the near infrared (NIR) wavelength region of 3.3 borosilicate glass capillaries with rectangular-section channel (Vitrotubes, VitroCom, New Jersey, USA) employed as micro-opto-fluidic devices for refractive index sensing.

A drawing of the capillary section is shown in the inset of Fig. 1. For 20-µm capillaries, the thickness t_f and t_b of the front and back glass wall, respectively, as well as the depth d of the internal gap were nominally equal to 20 µm whereas the width w of the flat side was w = 200 µm.

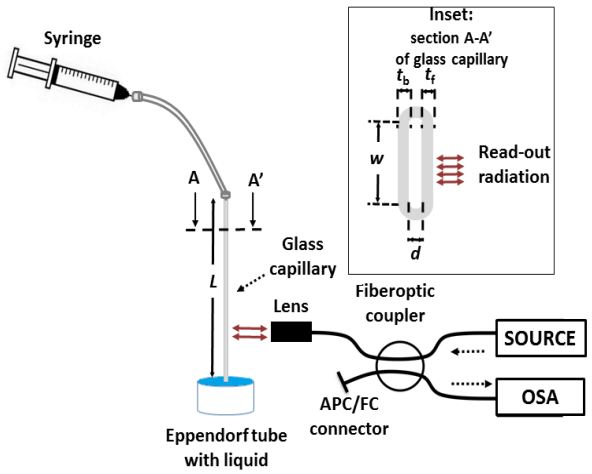

Fig. 1. Instrumental configuration for reflected optical power measurements on rectangular glass micro-capillaries. OSA: Optical Spectrum Analyzer; Lens: pigtail style focuser with aspheric lens; Source: Infrared radiation. Inset: view of capillary section.

For 50-µm capillaries, t_f = t_b = d = 50 µm (nominal values) and w = 500 µm. All tested capillaries were 50 mm long. The manufacturer ensures ±10% standard tolerance for the inner dimensions only of both kinds of capillary. The calculated total internal volume was approximately 200 nl for the 20-µm capillary and 1250 nl for the 50-µm capillary. During the opto-fluidic experiments, the capillary was securely fastened to a mechanical mounting placed on an x-y-z precision micropositioner. The capillary was connected upstream to a syringe by means of a luer-cone female adapter inserted in a plastic tube that was attached to the capillary with silicone glue. Capillary filling was achieved by dipping the free end of the capillary (downstream) into an Eppendorf tube containing the fluid to be tested. In most of the cases, fluids entered by capillary force and the syringe was used just to push air for emptying the capillary. Specifically, we used Glucose solutions in water at different concentrations (obtained by dilution from an injectable Glucose solution in water at 33%) and Bovine Serum Albumin (BSA) solutions in water, as test fluids. With regard to the optical and instrumental configuration a bidirectional 2x2 fiberoptic coupler with 50:50 coupling ratio and flat spectral response was used to carry broadband radiation toward the capillary and to redirect the back reflected light toward the monochromator input of an optical spectrum analyzer (OSA, Agilent 86142B, resolution bandwidth (RB) = 0.1 nm) [11]. A pigtail style focuser with aspheric lens (by OzOptics) connected at the output port of the coupler was used as readout termination, generating a low divergence 50-µm diameter beam on the capillary wall, that was placed at a working distance of about 23.5 mm.

The readout lens was secured on a kinematic mount for optics to allow the precise alignment of the readout beam in direction perpendicular to the flat side of the capillary, in order to maximize the signal coupled back to the detector. The use of a low numerical aperture lens

ensures that radiation due to Fresnel reflections at the interfaces is efficiently detected whereas interference effects due to scattered radiation are minimized. Moreover, exploitation of orthogonal incidence allows polarization insensitive measurements.

All fiber components were based on standard telecommunication optical fibers (9/125 μm core/cladding diameter). The unused output port of the coupler was terminated with an angled connector to avoid spurious back reflections.

Readout radiation was provided by two fiber-coupled amplified spontaneous emission (ASE) sources. We used a superluminescent emitting diode (SLED) with Gaussian emission spectrum with peak wavelength λ_p = 1.3 μm, Full-Width-Half-Maximum FWHM=75 nm, and power spectral density peak of approximately -20 dBm/0.1 nm (with pumping current I = 500 mA, temperature T=25 °C) as well as a diode-pumped Erbium-doped fiber source (EBS) with central wavelength λ_c = 1.55 μm, power spectral density of approximately -10 dBm/0.1 nm on a 45 nm bandwidth. Fiber pig-tailed optical isolators (OI) protected both sources from back reflections into the active medium.

III. Results and Discussion

A. *Investigation of 20-μm capillary*

We performed numerical simulations to investigate the dependence of the reflectivity spectrum of the capillary on the RI of the filling fluid. With this aim, we modeled the capillary as a three-layer structure corresponding to the front glass wall, the inner gap and the back wall, immersed in air [39]. Even though the reflectivity of a multilayer is often calculated by transfer matrix methods [40], in the case of the capillary a simple approach based on electromagnetic field propagation is sufficient. We considered each single layer of the capillary as a Fabry-Pérot etalon to obtain the spectral reflectivity function of the electric field, starting from the back glass wall [40]. By iteratively computing the reflectivity in backward direction with respect to the incident wave, the reflectivity of the whole structure can be calculated. The overall reflection response of the structure was thus obtained recursively by the propagation of the reflection responses of the various layers, as explained in the Appendix. In the model, we took into account the wavelength dependence of the RI of Borosilicate glass [42]; for distilled water we assumed n_{water} = 1.3225 RIU (RIU) at λ= 1.3 μm and n_{water} = 1.3180 RIU at λ = 1.55 μm [42].

Since the real sizes of the capillary are different form the nominal ones, the model was used for extracting the effective geometrical dimensions of the device that best fitted the experimental spectrum. Fig. 2a shows the theoretical reflectivity spectrum (red trace) calculated through least squares fitting of the experimental reflectivity collected on the 20-μm capillary filled with water (blue trace) using the SLED as readout source. In this case, the geometrical parameters provided by the numerical fitting with 95% confidence bounds were d = 21.18 μm, t_f = 17.52 μm and t_b = 17.03 μm.

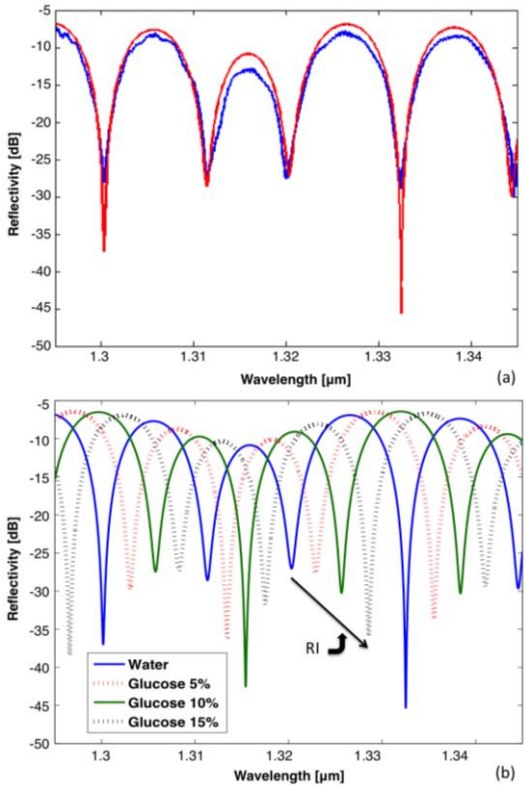

Fig. 2. Reflectivity spectra relative to 20-μm capillary using the SLED source. (a) Experimental results (blue trace) acquired on the capillary filled with water and calculated reflectivity (red trace) through numerical simulations (best fitting parameters d = 21.18 μm, t_f = 17.52 μm, t_f = 17.03 μm, with 95% confidence bounds). (b) Numerical results obtained using the best fitting parameters and considering Glucose solutions in water at 0% (blue trace), 5% (dotted red trace), 10% (green trace) and 15% (dotted gray trace) concentrations as filling fluid.

These data were in agreement with the actual thicknesses measured on that capillary sample by means of an interferometric setup [43]. The value of d is also in accordance with the standard tolerance ensured by the manufacturer. At this purpose, the refractive index n of the solutions was estimated [44] using the relation:

$$n = n_0 + \alpha \cdot C \quad (1)$$

where n_0 is the refractive index of the solvent (distilled water in our case), C is the concentration of the solute and $\alpha = dn/dC$ is the refractive index increment that is specific for each solute; for glucose, we assumed α = 0.145 cm^3/g [45]. The reflectivity spectra of the 20-μm capillary obtained numerically by considering Glucose solutions in water at 0%, 5%, 10% and 15% concentrations are reported in Fig. 2b. The refractive index increase due to the augmented Glucose concentration clearly induces a shift of the spectra toward longer wavelengths. This result could be qualitatively attained by considering the capillary as a Fabry-Pérot (FP) cavity.

However, the standard equations valid for this simplified model are not suitable for correctly describing the effect of RI changes on the spectral line-shape. For example, the shifts of the various minima are different for the same fluidic index change but do not follow a monotonic increase with wavelength. In particular, the hypothesis of constant reflectivity of the parallel plates limiting the FP cavity does not hold for the capillary as the reflectivity of the interfaces depends on the RI of the fluids into the channel and outside the capillary [39].

We then performed experimental investigation of the spectral response of the 20-µm capillary using Glucose solutions at different concentration and collecting the reflected power spectra with both SLED and EBS as readout sources in order to cover two different spectral ranges. Fig. 3a shows a sequence of experimental spectra, obtained with the SLED, relative to 15 increasing concentrations of Glucose in water, from 0% (distilled water) to 33%.

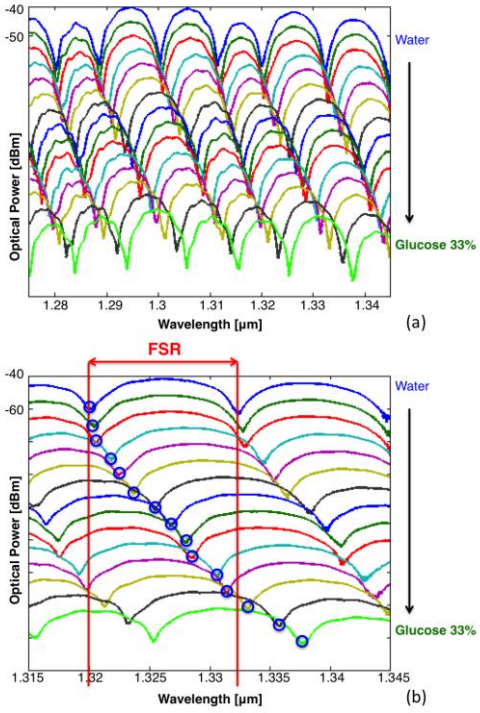

Fig. 3. Reflected power spectra measured with the SLED on a 20-µm capillary filled with Glucose solutions in water at 15 different concentrations (0%, 0.5%, 1%, 3%, 5%, 7%, 10%, 12%, 15%, 16.5%, 20%, 22%, 25%, 30%, 33%). (a) Full SLED bandwidth; traces are vertically separated by 5 dB for better visualization. (b) Zoom of the same spectra in (a) on a 30-nm bandwidth; Traces in (b) are vertically separated by 10 dB. For both (a) and (b), RB = 0.1 nm, spectral step = 20 pm. The absolute scale, on the y-axis, refers only to the spectrum relative to water.

As predicted by the numerical simulations, the refractive index increase due to the augmented Glucose concentration induces a shift of the reflected spectrum toward longer wavelengths. In Fig. 3b, a zoom of the acquired spectra over a narrower wavelength range (20 nm) is reported. On the spectrum relative to water filling we highlight the Free Spectral Range (FSR), *i.e.*, the wavelength interval between two adjacent minima: for the 20-µm capillary at λ = 1.3 µm we obtained FSR ≈ 12 nm. FSR is an important parameter since it defines the largest spectral shift that can be correlated to a refractive index change without ambiguity. As shown in Fig. 3b, the shifts due to 25%, 30% and 33% Glucose solutions were larger than a FSR.

Fig. 4 shows a sequence of spectra measured on the same capillary with the EBS source relative to different Glucose solutions in water. In this wavelength range we found FSR = 14 nm, slightly wider then the one obtained with the SLED source; only the spectra relative to 30% and 33% concentrations were shifted by more than 14 nm with respect to water.

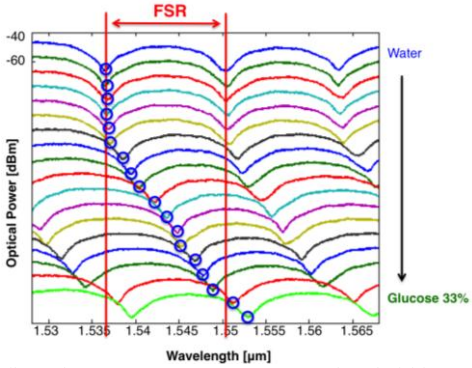

Fig. 4. Reflected power spectra on a 40-nm bandwidth measured with the EBS source on a 20-µm capillary filled with Glucose solutions in water at 18 different concentrations (from 0% up to 33%). Traces are vertically translated by 10 dB. RB=0.1 nm, spectral step = 50 pm.

In order to obtain the experimental refractive index sensitivity, from the spectral data acquired on the same 20-µm capillary with both light sources we derived the wavelength position λ_{min} of the minima as a function of the estimated RI of the tested solutions, plotted in Fig. 5 to obtain the calibration curve of the sensor as function of wavelength.

The graph in Fig. 5a illustrates the shift toward longer wavelengths of one reflectivity notch, initially detected at λ = 1320.1 nm when water is filling the capillary, induced by refractive index variations due to the increasing Glucose concentration.

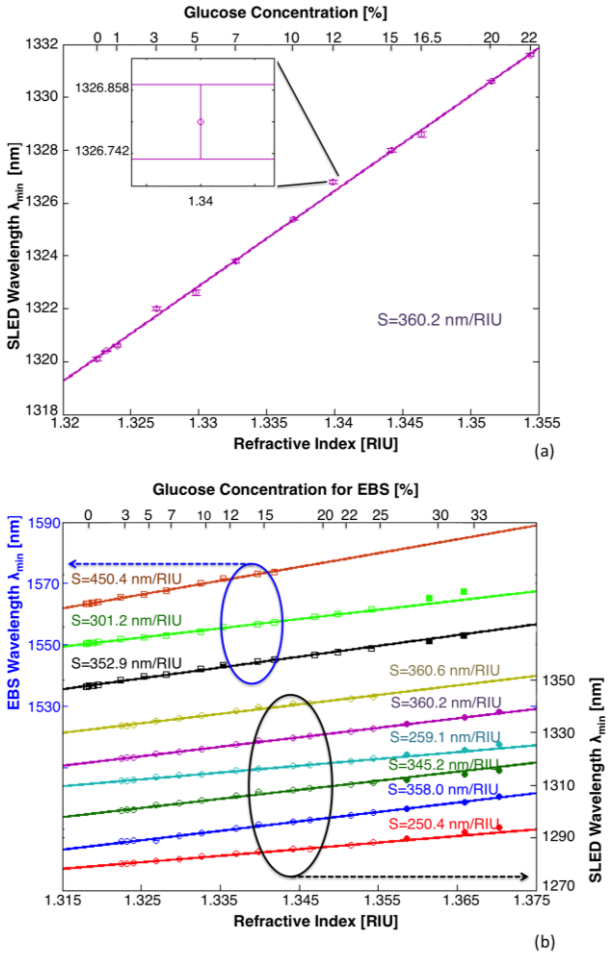

Fig. 5. Calibration curves of a 20-µm capillary as refractive index sensor. (a) Mean values with error bars of the wavelength position of the reflectivity notch (found at λ = 1320.1 nm when water is filling the capillary) as a function of the refractive index of the tested Glucose solutions. The zoom in the inset highlights the presence of error bars. The sensitivity S is obtained as the slope of the line fitting the data points (R^2=0.9984). (b) Mean values with error bars of the wavelength position of all detected experimental minima as a function of the refractive index of the tested Glucose solutions. Data relative to the wavelengths within a FSR are reported using empty markers, whereas filled markers represent data outside a FSR. Glucose solutions in water at concentration of 0%, 0.1%, 0.3%, 0.5%, 0.7%, 1%, 3%, 5%, 7%, 10%, 12%, 15%, 16.5%, 20%, 22%, 25%, 30%, and 33% were used for the experiment with the EBS. Concentrations of glucose in water of 0%, 0.5%, 1%, 3%, 5%, 7%, 10%, 12%, 15%, 16.5%, 20%, 22%, 25%, 30%, and 33% were used for the experiment with the SLED. Linear fitting of data points within a FSR evaluates the sensitivity of each minimum.

Error bars superposed to the data markers are estimated on the basis of the calculated standard deviation (that were obtained as a result of at least three measurements) and remain in all experiments within a few hundreds of pm. Recalling that the sensitivity (S) is defined as the spectral shift induced for a given refractive index variation or $S = d\lambda_{min}/dn$, by linear fitting the data (only within a FSR) the sensitivity was calculated for each minimum. The best value S = 450.4 nm/RIU (with coefficient of determination (R^2) equal to 0.9976) was obtained by following the shift of the reflectivity notch starting (in presence of water) from about λ = 1563.3 nm (EBS source) whereas the best value obtained using the SLED was S = 360.6 nm/RIU (R^2 = 0.9926) following λ_{min} from 1322.5 nm. As numerically predicted, the minima have different sensitivities. Another important parameter in view of the application of the proposed system as refractive index sensor is the limit of detection (*LoD*), which indicates the smallest measurable RI change. *LoD* can be calculated [8] as:

$$LoD = R / S \qquad (2)$$

where R is the system resolution that is usually defined as 3σ with σ the standard deviation of the experimental data.

Values of *LoD* calculated for each reflectivity minima (detected in the presence of water, as reference fluid, inside the capillary) were found in the range from $4.8\cdot10^{-4}$ to $1.2\cdot10^{-3}$ RIU with the SLED and from $5.7\cdot10^{-4}$ to $1.3\cdot10^{-3}$ RIU with the EBS.

For comparison, we extracted the theoretical sensitivity (S_t) from the simulated spectra. As an example, following the shift of the reflectivity notch starting from λ = 1299 nm in presence of water, we attained S_t = 353.7 nm/RIU (R^2 = 0.9991) in agreement with the experimental value S = 345.2 nm/RIU (R^2 = 0.9932) obtained for the same minimum. In the EBS band, following the notch at 1563 nm, we found a theoretical sensitivity S_t = 465.1 nm/RIU (R^2 = 0.9999) slightly higher than the corresponding experimental value S = 450.4 nm/RIU (R^2 = 0.9976).

B. Investigations of 50-µm capillary

We tested rectangular capillaries with internal dimension of 50 µm x 500 µm with Glucose solutions as well as BSA solutions in water. Fig. 6 shows a sequence of reflected power spectra acquired on a 50-µm capillary using EBS, relative to 11 different concentrations of Glucose in water, from 0% to 10%, where the FSR = 6 nm is also highlighted.

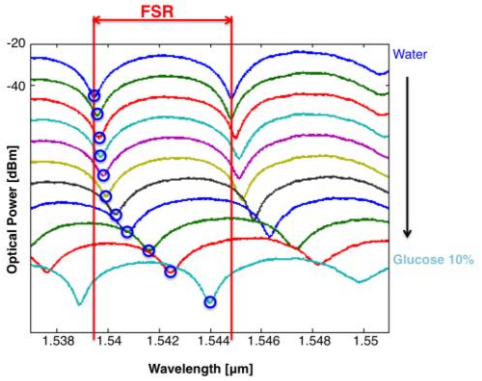

Fig. 6. Reflected power spectra on a 14-nm bandwidth collected using the EBS source on a 50-µm capillary filled with Glucose solutions in water at 11 different concentrations (0%, 0.1%, 0.3%, 0.5%, 0.7%, 1%, 2%, 3%, 5%, 7%, 10%). Traces are vertically separated by 10 dB for clarity. The absolute scale, on the y-axis, refers only to the spectrum relative to water. RB = 0.1 nm, spectral step = 25 pm.

As theoretically expected, the FSR provided by the 50-µm devices was narrower then that achieved with the

20-µm capillary in the same wavelength region, very likely due to the wider inner channel and the thicker walls of the 50-µm capillary. The SLED was not used for readout since at shorter wavelengths the FSR would have been even narrower.

We then report in Fig. 7 the mean values of λ_{min} as a function of the refractive indices for all the detected reflectivity notches: the standard deviation (for error bars) was found between 10^{-6} µm and 10^{-4} µm. Also on these data, linear fitting provided the RI sensitivity. The best value $S = 351.9$ nm/RIU was obtained by following the shift of the minimum starting at $\lambda = 1561$ nm and *LoD* values in the range from $2.46 \cdot 10^{-5}$ to $3.27 \cdot 10^{-4}$ RIU were demonstrated.

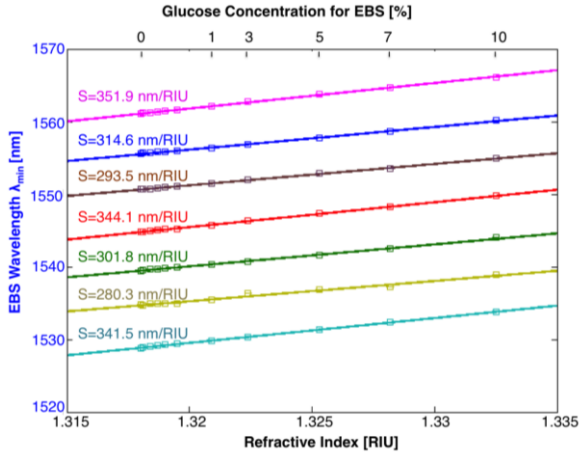

Fig. 7. Mean values of the wavelength position of the experimental minima with error bars as a function of the refractive index of the tested Glucose solutions. Linear fitting provides the sensitivity.

By running numerical simulations, least squares fitting of the reflectivity relative to water yielded $t_f = 52.25$ µm, $t_b = 51.95$ µm, and $d = 50.14$. Again, these values were in agreement with the measured thicknesses [43]. Then, with these parameters a theoretical sensitivity $S_t = 359.5$ nm/RIU ($R^2 = 0.9998$) was calculated for the minimum at $\lambda = 1529$ nm, in accordance with the corresponding experimental value $S = 341.5$ nm/RIU ($R^2 = 0.9995$).

Further testing was performed on another sample of 50-µm capillary using BSA solutions. Fig. 8 reports a sequence of reflected power spectra acquired using EBS and relative to 8 different concentrations of BSA in water, from 0% up to 7%.

The wavelength shift of all the detected minima on the EBS emission bandwidth is finally reported in Fig. 9 as a function of the RI to obtain the experimental sensitivity by linear fitting.

Refractive indices of the tested solutions were estimated from (1), assuming $\alpha = 0.183$ g/cm^3 [45], [46]. The best experimental sensitivity was about $S = 350$ nm/RIU whereas the worst *LoD* was of the order of 10^{-5} RIU. In this case, the numerical simulation provided a theoretical sensitivity $S_t = 340.1$ nm/RIU ($R^2 = 0.9987$) at $\lambda = 1566$ nm similar to the experimental value $S = 329.8$ nm/RIU ($R^2 = 0.9986$).

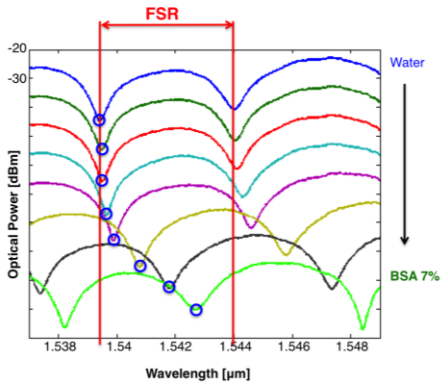

Fig. 8. Reflected power spectra on a 12-nm bandwidth collected with EBS on a 50-µm capillary filled with BSA solutions in water at different concentrations (0%, 0.1%, 0.3%, 0.5%, 1%, 3%, 5%, 7%). Traces are vertically separated by 10 dB for clarity. The absolute scale, on the y-axis, refers only to the spectrum relative to water. RB = 0.1 nm and spectral step = 25 pm.

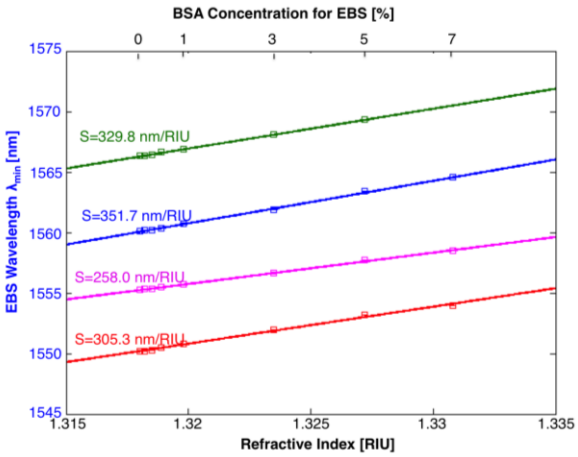

Fig. 9. Mean values of the wavelength position of the experimental minima with error bars as a function of the refractive index of the tested BSA solutions in water. Linear fitting provides the sensitivity.

IV. Conclusions

In this work, we demonstrated the use of low-cost glass micro-capillaries with rectangular cross-section for the realization of RI micro-opto-fluidic sensors. Both capillary sizes (50 µm and 20 µm) provided RI sensitivities greater than 250 nm/RIU, *LoD*s in the range of 10^{-5}-10^{-3} RIU and linear response with all tested solutions.

Numerical simulations performed by modeling the device as a three-layer structure yielded results in good agreement with the experimental data, thus confirming and validating our measurements. The proposed instrumental configuration and readout method allows performing remote optical measurements without any contact between the optical components and the capillary, which can be easily removed and replaced without affecting the optical setup. The optical method employed for RI detection is based on the shift of the wavelength position of reflectivity minima and was demonstrated using broadband light sources and the OSA for detection. Similar responses could be attained with a tunable source and a photodetector. Moreover, measuring the variation

of the reflected light intensity at two or more wavelengths could achieve direct monitoring of RI changes in the time domain.

Sensitivities and *LoD* obtained using off-the-shelf and low-cost devices are comparable with data found in the literature relative to optical devices realized with specific micro-fabrication techniques. Glass rectangular micro-capillaries represent an interesting solution for the implementation of low-cost devices for (bio)sensing, applicable for example in the field of clinical analyses where disposable devices are preferred, removing the risk of cross-contaminations. For biological analyses the proposed system offers further advantages: rectangular capillaries could be easily integrated in micro-fluidic system, allowing repeatable and fast measurements, and the use of infrared radiation is minimally invasive for biological substances. Moreover, active and passive optical components suitable for the infrared spectral region are commercially available as they are already used in the field of optical communications.

Future developments will consist in realizing specific adapters and connectors for interfacing the capillaries with macro-fluidic devices using micro-fabrication techniques, or even better 3D printing, for shaping polymeric materials.

The demonstrated sensors are volumetric, since the response of the device depends on the RI of the medium inserted in the capillary channel. Functionalization of the internal surfaces with bioreceptors could be exploited for creating specific biosensors, where surface RI changes would be induced by the occurrence of a binding reaction. Glass capillaries are good candidates for such application as glass functionalization techniques are well known and easily performed.

APPENDIX

MODEL FOR NUMERICAL CALCULATION OF THE SPECTRAL REFLECTIVITY

The capillary can be considered as a multilayer structure composed by alternating dielectric materials with different refractive indexes and thicknesses along a single axis (one-dimensional structure), since the beam diameter is always smaller than the width/length of the flat side of the capillary. Even though the reflectivity of this kind of structures is often calculated by transfer matrix methods, which can be eventually generalized for two- and three-dimensional structures, we selected an approach based on electromagnetic field propagation for the sake of simplicity since we are only interested in describing a one-dimensional structure composed by three different layers immersed in air. This approach considers the electric field propagation across the capillary modeled as a cascade of Fabry-Perot etalons, as shown in Figure 10.

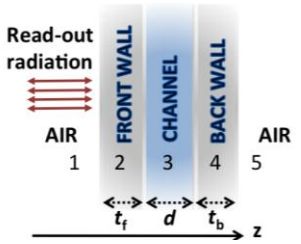

Fig. 10. Schema of the capillary interfaces, used for numerical simulations.

Starting with considering the layer of the back glass wall of the capillary, we can identify two interfaces: 3-4 between channel (3) and back glass wall (4) and 4-5 between back glass-wall (4) and air (5). We assume that t_b is the thickness of the back wall, n_{glass} is the refractive index of glass, n is the refractive index of the fluid in the channel and $n_{air} = 1$. We also assume a plane wave propagating in the z-direction perpendicular to the interfaces. If we define the field reflection (ρ) and transmission (τ) coefficients for the wave propagating through the interfaces as:

$\rho_{3\text{-}4} = (n - n_{glass}) / (n + n_{glass}) = - \rho_{4\text{-}3}$

$\rho_{4\text{-}5} = (n_{glass} - n_{air}) / (n_{glass} + n_{air}) = (n_{glass} - 1) / (n_{glass} + 1)$

$\tau_{3\text{-}4} = 2n / (n + n_{glass})$

$\tau_{4\text{-}3} = 2n_{glass} / (n_{glass} + n)$,

the electric field reflection coefficient $\rho_{3\text{-}4'}$ of the whole glass back-wall, considered as an overall equivalent interface 3-4', can be calculated as:

$$\rho_{3\,4'} = \rho_{3\,4} + \frac{\tau_{3\,4}\,\tau_{4\,3}\,\rho_{4\,5}\exp(-\mathrm{j}2kn_{glass}t_b)}{1-\rho_{4\,3}\,\rho_{4\,5}\exp(-\mathrm{j}2kn_{glass}t_b)}$$

where $k = 2\pi / \lambda$.

By iteratively computing the electric field reflection coefficient in the backward direction with respect to the incident wave, the reflectivity of the capillary can be calculated. By considering the layer of the capillary channel, we can now identify two interfaces: 2-3 between front glass wall (2) and channel (3) and 3-4' between channel (3) and equivalent medium 4'. We assume here that d is the channel depth. The electric field reflection coefficient $\rho_{2\text{-}3'}$ at the overall equivalent interface 2-3' is given by:

$$\rho_{2\,3'} = \rho_{2\,3} + \frac{\tau_{2\,3}\,\tau_{3\,2}\,\rho_{3\,4'}\exp(-\mathrm{j}2knd)}{1-\rho_{3\,2}\,\rho_{3\,4'}\exp(-\mathrm{j}2knd)}$$

where

$\rho_{2\text{-}3} = (n_{glass} - n) / (n_{glass} + n) = - \rho_{3\text{-}2}$

$\tau_{2\text{-}3} = 2n_{glass} / (n_{glass} + n)$

$\tau_{3\text{-}2} = 2n / (n + n_{glass})$.

Finally, assuming that t_f is the thickness of the front wall, in analogy with the previous steps, the electric field reflection coefficient of the whole capillary $\rho_{1\text{-}2'}$ is given by:

$$\rho_{1\,2'} = \rho_{1\,2} + \frac{\tau_{1\,2}\,\tau_{2\,1}\,\rho_{2\,3'}\exp(-\mathrm{j}2kn_{glass}t_f)}{1-\rho_{2\,1}\,\rho_{2\,3'}\exp(-\mathrm{j}2kn_{glass}t_f)}$$

where $\rho_{1\text{-}2} = (1 - n_{glass}) / (1 + n_{glass}) = - \rho_{2\text{-}1}$,

$\tau_{1\text{-}2} = 2 /(1 + n_{glass})$, $\tau_{2\text{-}1} = 2\, n_{glass} / (n_{glass} + 1)$.

The spectral reflectivity R (*e.g.*, reported in Figure 1b) is then

obtained by plotting $|\rho_{1\text{-}2'}|^2$ in dB as a function of the wavelength λ. Best fitting procedure was performed by least square method comparing experimental and numerical results.

ACKNOWLEDGMENT

This research was partially funded by the Fondazione CARIPLO, Grant no. 2011-0308. The authors wish to thank Dr. G. Mazzini for providing BSA solutions and for fruitful discussions.

REFERENCES

[1] G. M. Whitesides, "The origins and the future of microfluidics," *Nature*, vol. 442, no. 7101, pp. 368–73, Jul. 2006.
[2] D. Psaltis, S. R. Quake, and C. Yang, "Developing optofluidic technology through the fusion of microfluidics and optics," *Nature*, vol. 442, no. 7101, pp. 381–6, Jul. 2006.
[3] K. B. Mogensen and J. P. Kutter, "Optical detection in microfluidic systems," *Electrophoresis*, vol. 30 Suppl1 , pp. S92–S100, Jun.2009.
[4] X. Fan and I. M. White, "Optofluidic microsystems for chemical and biological analysis," *Nat. Photonics*, vol. 5, no. 10, pp. 591–7, Oct. 2011.
[5] V. R. Horowitz, D. D. Awschalom, and S. Pennathur, "Optofluidics: field or technique?," *Lab Chip*, vol. 8, no.11, pp. 1856–63, Nov.2008.
[6] N. M. M. Pires, T. Dong, U. Hanke, and N. Hoivik, "Recent developments in optical detection technologies in lab-on-a-chip devices for biosensing applications," *Sensors*, vol. 14, no. 8, pp. 15458–79, Jan. 2014.
[7] H. K. Hunt and A. M. Armani, "Label-free biological and chemical sensors," *Nanoscale*, vol. 2, no. 9, pp. 1544–59, Sep. 2010.
[8] I. M. White and X. Fan, "On the performance quantification of resonant refractive index sensors," *Opt. Express*, no. 1–2, pp. 117–27, Aug. 2008.
[9] G. Barillaro, S. Merlo, S. Surdo, L. M. Strambini, and F. Carpignano, "Integrated optofluidic microsystem based on vertical high-order one-dimensional silicon photonic crystals," *Microfluid. Nanofluidics*, vol. 12, no. 1–4, pp. 545–52, Nov. 2011.
[10] S. Surdo, S. Merlo, F. Carpignano, L. M. Strambini, C. Trono, A. Giannetti, F. Baldini, and G. Barillaro, "Optofluidic microsystems with integrated vertical one-dimensional photonic crystals for chemical analysis," *Lab Chip*, vol. 12, no. 21, pp. 4403–15, Oct. 2012.
[11] S. Surdo, F. Carpignano, L. M. Strambini, S. Merlo, and G. Barillaro, "Capillarity-driven (self-powered) one-dimensional photonic crystals for refractometry and (bio)sensing applications," *RSC Adv.*, vol. 4, no. 94, pp. 51935–41, Sep. 2014.
[12] M. R. Lee and P. M. Fauchet, "Two-dimensional silicon photonic crystal based biosensing platform for protein detection," *Opt. Express*, vol. 15, no. 8, pp. 4530–35, Apr. 2007.
[13] P. S. Nunes, N. A. Mortensen, J. P. Kutter, and K. B. Mogensen, "Photonic crystal resonator integrated in a microfluidic system," *Opt. Lett.*, vol. 33, no. 14, pp. 1623–5, Jul. 2008.
[14] S. Mandal, J. M. Goddard, and D. Erickson, "A multiplexed optofluidic biomolecular sensor for low mass detection," *Lab Chip*, vol. 9, no. 20, pp. 2924–32, Oct. 2009.
[15] S. Mandal and D. Erickson, "Nanoscale optofluidic sensor arrays," *Opt. Express*, vol. 16, no. 3, p. 1623, 2008.
[16] W. C. L. Hopman, P. Pottier, D. Yudistira, J. Van Lith, P. V Lambeck, R. M. D. La Rue, A. Driessen, H. J. W. M. Hoekstra, and R. M. De Ridder, "Quasi-one-dimensional photonic crystal as a compact building-block for refractometric optical sensors," *IEEE J. Sel. Top. Quantum Electron.*, vol. 11, no. 1, pp. 11–6, 2005.
[17] A. A. P. Trichet, J. Foster, N. E. Omori, D. James, P. R. Dolan, G. M. Hughes, C. Vallance, and J. M. Smith, "Open-access optical microcavities for lab-on-a-chip refractive index sensing," *Lab Chip*, vol. 14, no. 21, pp. 4244–9, Nov. 2014.
[18] V. M. N. Passaro, B. Troia, M. La Notte, and F. De Leonardis, "Photonic resonant microcavities for chemical and biochemical sensing," *RSC Adv.*, vol. 3, no. 1, p. 25, 2013.
[19] T. Ling and L. J. Guo, "A unique resonance mode observed in a prism-coupled micro-tube resonator sensor with superior index sensitivity," *Opt. Express*, vol. 15, no. 25, p. 17424, 2007.
[20] M. Huang, A. A. Yanik, and T. Chang, "Sub-wavelength nanofluidics in photonic crystal sensors," *Opt. Express*, vol. 17, no. 31, pp. 5742–7, 2009.
[21] E. Chow, A. Grot, L. W. Mirkarimi, M. Sigalas, and G. Girolami, "Ultracompact biochemical sensor built with two-dimensional photonic crystal microcavity," *Opt. Lett.*, vol. 29, no. 10, pp. 1093–5, May 2004.
[22] C. A. Barrios, M. J. Bañuls, V. González-Pedro, K. B. Gylfason, B. Sánchez, A. Griol, A. Maquieira, H. Sohlström, M. Holgado, and R. Casquel, "Label-free optical biosensing with slot-waveguides," *Opt. Lett.*, vol. 33, no. 7, p. 708, Mar. 2008.
[23] H. Li and X. Fan, "Characterization of sensing capability of optofluidic ring resonator biosensors," *Appl. Phys. Lett.*, vol. 97, no. 1, p. 011105, 2010.
[24] G. Testa, Y. Huang, P. M. Sarro, L. Zeni, and R. Bernini, "Integrated silicon optofluidic ring resonator," *Appl. Phys. Lett.*, vol. 97, no. 13, p. 131110, 2010.
[25] C. Ciminelli, C. M. Campanella, F. Dell'Olio, C. E. Campanella, and M. N. Armenise, "Label-free optical resonant sensors for biochemical applications," *Prog. Quantum Electron.*, vol. 37, no. 2, pp. 51–107, Mar. 2013.
[26] Y. Kimura, T. G. Henares, S. Funano, T. Endo, and H. Hisamoto, "Open-type capillary-assembled microchip for rapid, single-step, simultaneous multi-component analysis of serum sample," *RSC Adv.*, vol. 2, no. 25, p. 9525, 2012.
[27] A. Yalcin and K. Popat, "Optical sensing of biomolecules using microring resonators," *IEEE J. Sel. Top. Quantum Electron.*, vol. 12, no. 1, pp. 148–55, 2006.
[28] M. Iqbal, M. A. Gleeson, B. Spaugh, F. Tybor, W. G. Gunn, M. Hochberg, T. Baehr-jones, R. C. Bailey, and L. C. Gunn, "Label-free biosensor arrays based on silicon ring resonators and high-speed optical scanning instrumentation," *IEEE J. Sel. Top. Quantum Electron.*, vol. 16, no. 3, pp. 654–61, 2010.
[29] X. Zhou, L. Zhang, and A. Armani, "On-chip biological and chemical sensing with reversed fano lineshape enabled by embedded microring resonators," *IEEE J. Sel. Top. Quantum Electron.*, vol. 20, no. 3, p. 5200110, 2014.
[30] R. St-Gelais, J. Masson, and Y. A. Peter, "All-silicon integrated Fabry–Pérot cavity for volume refractive index measurement in microfluidic systems," *Appl. Phys. Lett.*, vol. 94, no. 24, p. 243905, 2009.
[31] Y. Guo, H. Li, K. Reddy, H. S. Shelar, V. R. Nittoor, and X. Fan, "Optofluidic Fabry-Pérot cavity biosensor with integrated flow-through micro-/nanochannels," *Appl. Phys. Lett.*, vol. 98, no. 4, p. 041104, 2011.
[32] T. Tsuda, J. V. Sweedler, and R. N. Zare, "Rectangular capillaries for capillary zone electrophoresis," *Anal. Chem.*, vol. 62, no. 19, pp. 2149–52, Oct. 1990.
[33] B. Hammarström, M. Evander, H. Barbeau, M. Bruzelius, J. Larsson, T. Laurell, and J. Nilsson, "Non-contact acoustic cell trapping in disposable glass capillaries," *Lab Chip*, vol. 10, no. 17, pp. 2251–2257, 2010.
[34] M. Evander and M. Tenje, "Microfluidic PMMA interfaces for rectangular glass capillaries," *J. Micromechanics Microengineering*, vol. 24, no. 2, p. 027003, 2014.
[35] J. 0. Harris, "Techniques and experiments," 1975.
[36] Y. Zhu and K. Petkovic-Duran, "Capillary flow in microchannels," *Microfluid. Nanofluidics*, vol. 8, no. 2, pp. 275–82, Nov.2009.
[37] X. Yang, O. Forouzan, J. M. Burns, and S. S. Shevkoplyas, "Traffic of leukocytes in microfluidic channels with rectangular and rounded cross-sections," *Lab Chip*, vol. 11, no. 19, pp. 3231–3240, 2011.
[38] P. R. Waghmare and S. K. Mitra, "A comprehensive theoretical model of capillary transport in rectangular microchannels," *Microfluid. Nanofluidics*, vol. 12, no. 1–4, pp. 53–63, Jul. 2011.
[39] M. Born and E. Wolf, *Principles of Optics*. Oxford, UK:Pergamon Press, UK, 1986.
[40] S. J. Orfanidis, "Multilayer structures," in *Electromagnetic Waves and Antennas*. 2014, Cap. 6, pp. 186–234.
[41] G. Barillaro, L. M. Strambini, V. Annovazzi-Lodi, and S. Merlo, "Optical characterization of high-order 1-D silicon photonic crystals," *IEEE J. Sel. Top. Quantum Electron.*, vol. 15, no. 5, pp. 1359–67, 2009.
[42] "RefractiveIndex," *http://refractiveindex. info*. [Online]. Available: http://refractiveindex.info. [Accessed: 01-Oct-2014].
[43] F. Carpignano, G. Rigamonti, and S. Merlo, "Characterization of rectangular glass microcapillaries by low-choerence reflectometry," *IEEE Photonics Technol. Lett.*, vol. 27, no. 10, pp. 1064–7, 2015.
[44] P. L. Gourley, "Biocavity laser for high-speed cell and tumour biology," *J. Phys. D. Appl. Phys.*, vol. 36, no. 14, pp. R228–39, 2003.

[45] T. Tumolo, L. Angnes, and M. S. Baptista, "Determination of the refractive index increment (dn/dc) of molecule and macromolecule solutions by surface plasmon resonance," *Anal. Biochem.*, vol. 333, no. 2, pp. 273–9, Oct. 2004.
[46] D. Fu, W. Choi, Y. Sung, S. Oh, Z. Yaqoob, Y. Park, R. R. Dasari, and M. S. Feld, "Ultraviolet refractometry using field-based light scattering spectroscopy," *Opt. Express*, vol. 17, no. 21, pp. 18878–86, Oct. 2009.

Francesca Carpignano was born in Broni (PV), Italy, in 1985. She received the Graduate degree (*cum laude*) in biomedical engineering from the University of Pavia, Italy, in 2010, with a thesis on micro-opto-fluidic devices for photonic crystal biosensors and the Ph.D. degree in bioengineering and bioinformatics from the same university in 2014 with a dissertation on a new 3-D silicon microstructure for simultaneous cell culture and label-free optical transduction. Her current research interests include biosensors, microfluidics, photonic crystals, silicon micromachined devices, lab-on-chip, nanomedicine, and cell culture. She is the coauthor of more than 40 publications in journals, books, and conference proceedings.

Giulia Rigamonti was born in Ponte dell'Olio (PC), Italy, in 1989. She received the Graduate degree in bioengineering from the University of Pavia, Italy, in 2014, with a thesis on micro-opto-fluidic devices based on rectangular glass micro-capillaries for the detection of fluids of biological interest. Currently, she is a Ph.D. student at the same university.

Tommaso Migliazza was born in Catanzaro (CZ), Italy, in 1989. He received the Graduate degree in bioengineering from University of Pavia, Italy, in 2014, with a thesis on micro-opto-fluidic devices as refractive index sensors for biological application.

Sabina Merlo (M'01–SM'05) was born in Pavia, Italy, in 1962 and received the degree in electronic engineering from the University of Pavia in 1987. She received a Rotary Foundation Graduate Scholarship for study at the University of Washington, Seattle, WA, USA, and received the M.S.E. degree in bioengineering in 1989 from the same university. She received the Ph.D. degree in electronic engineering from the University of Pavia in 1991. In 1993, she became an Assistant Professor and, in 2001, she became an Associate Professor in the Department of Electronics (now Dipartimento di Ingegneria Industriale e dell'Informazione), University of Pavia. Her main research interests include optical measurements on silicon micromachined devices (MEMS, MOEMS, photonic crystals), optical interferometry, chaos in lasers, fiber-optic passive components and sensors, and optical biosensors. She holds four patents and is the coauthor of more than 150 publications in journals, books and conference proceedings. She is an Associate Editor of the Journal of Microelectromechanical systems.
Dr. Merlo is a Member of AEIT, and Senior Member of the IEEE-Photonics Society.